Available online at www.sciencedirect.com
SCIENCE DIRECT®
Remote Sensing of Environment 91 (2004) 114–127
Remote Sensing of Environment
www.elsevier.com/locate/rse

Evaluation of the MODIS LAI algorithm at a coniferous forest site in Finland

Yujie Wang[a,*], Curtis E. Woodcock[a], Wolfgang Buermann[a], Pauline Stenberg[b], Pekka Voipio[c], Heikki Smolander[c], Tuomas Häme[d], Yuhong Tian[a], Jiannan Hu[a], Yuri Knyazikhin[a], Ranga B. Myneni[a]

[a] Department of Geography, Boston University, Boston, MA 02215, USA
[b] Department of Forest Ecology, University of Helsinki, FIN-00014, Finland
[c] Finnish Forest Research Institute, Suonenjoki Research Station, FIN-77600, Suonenjoki, Finland
[d] VTT Automation, Remote Sensing Group, FIN-02044 VTT, Finland

Received 8 July 2003; received in revised form 2 February 2004; accepted 14 February 2004

Abstract

Leaf area index (LAI) collected in a needle-leaf forest site near Ruokolahti, Finland, during a field campaign in June 14–21, 2000, was used to validate Moderate Resolution Imaging Spectroradiometer (MODIS) LAI algorithm. The field LAI data was first related to 30-m resolution Enhanced Thermal Mapper Plus (ETM+) images using empirical methods to create a high-resolution LAI map. The analysis of empirical approaches indicates that preliminary segmentation of the image followed by empirical modeling with the resulting patches, was an effective approach to developing an LAI validation surface. Comparison of the aggregated high-resolution LAI map and corresponding MODIS LAI retrievals suggests satisfactory behavior of the MODIS LAI algorithm although variation in MODIS LAI product is higher than expected. The MODIS algorithm, adjusted to high resolution, generally overestimates the LAI due to the influence of the understory vegetation. This indicates the need for improvements in the algorithm. An improved correlation between field measurements and the reduced simple ratio (RSR) suggests that the shortwave infrared (SWIR) band may provide valuable information for needle-leaf forests.

Keywords: MODIS LAI; Coniferous forest site; Finland

1. Introduction

Leaf area index (LAI) is a critical variable for understanding the biological and physical processes associated with vegetated land surfaces, and thus is a key input of climate and large-scale ecosystem models (Bonan, 1996; Dickinson et al., 1986; Foley et al., 1998; Sellers et al., 1997). LAI is defined as one-sided green leaf area per unit ground area in broadleaf canopies and as the hemisurface needle leaf area in coniferous canopies (Chen & Black, 1992; Knyazikhin et al., 1998a; Stenberg, 1996). For effective use in global-scale models, this variable must be collected over a long period of time and should represent every region of the terrestrial surface. LAI is operationally produced from MODerate Resolution Imaging Spectroradiometer (MODIS) data. The Terra platform, with MODIS and other instruments, was launched in December 1999 and data collection began in March 2000. The LAI products are at 1-km resolution at an 8-day interval. The product was made public in August 2000 through the Earth Resources Observation System (EROS) Data Center Distributed Active Archive Center. Presently, the emphasis within the MODIS program is on validation of the algorithm and its products (Privette et al., 2002).

Global validation of moderate- to coarse-resolution LAI products is a complicated and challenging task. It involves field measurements at sites representative of a wide range of vegetation types and scaling of field measurements from small areas to the resolution of satellite data. In addition, one should account for uncertainties in inputs to the retrieval

* Corresponding author. Goddard Earth Sciences and Technology Center, University of Maryland, Baltimore County, 1450 South Rolling Rd. Rm. 3.002, Baltimore, MD 21227, USA. Tel.: +1-301-614-6494; fax: +1-410-455-8806.
E-mail address: yujie@umbc.edu (Y. Wang).

0034-4257/$ - see front matter © 2004 Elsevier Inc. All rights reserved.
doi:10.1016/j.rse.2004.02.007

techniques due to uncertainties in registration, correction for atmosphere effects, etc., which make the comparison of ground-based measurements with coarse-resolution data a complicated task. The development of appropriate ground-based sampling strategies is critical to an accurate specification of uncertainties in the LAI product (Tian et al., 2002c).

A lot of efforts have been made to validate MODIS products. A system of land validation core sites that represent a range of biome types has been established (Morisette et al., 2002). At most of these sites, there is a long-term measurement program to support in situ measurements that can be used to assess the quality of MODIS land data products. One important project of all these validation efforts is BigFoot (Running et al., 1999). This project includes nine flux tower sites from Alaska to Brazil, each one represents one or two distinct biomes and collects field-based data over 5 × 5-km area around the tower. The result has been used as an independent evaluation of the quality of MODIS products (Cohen et al., 2003).

In this study, we will evaluate the MODIS LAI product which includes (a) creation of a 30-m resolution LAI map using data from a field campaign in Ruokolahti, Finland, and 30-m Landsat Enhanced Thermal Mapper Plus (ETM+) images, and (b) comparison of the MODIS LAI map with the fine-resolution LAI map aggregated to the MODIS resolution.

2. Experiment descriptions

2.1. Validation site and sampling strategy

A 1 × 1-km area of needle leaf forest near Ruokolahti, Finland (61.32°N, 28.43°E), was chosen for field data collection to validate the MODIS LAI product. The site is mostly occupied by Scots pine (*Pinus sylvestris*) and Norway spruce (*Pices abies*), with pines dominant. The Ruokolahti Forest site is a typical northern needle leaf forest, mixed with large and small lakes. The height of the trees was between 5 and 20 m. However, there was a small open area in this 1 × 1-km site, which was occupied by a mixture of re-growing smaller (less than 1.5 m in height) pine trees, dwarf shrubs and an understory of grasses. The 1 × 1-km site was divided into 20 rows and 20 columns, for a total 400 grid points. Each point was 50 m apart. Additionally, the canopy was stratified into sparse, intermediate and dense needle forests based on examination of an airborne 2-m resolution Charge-Couple Device (CCD) image. The CCD image has been manually registered to the ground using ground control points and auxiliary maps. The sparse forest is represented by the area mentioned above with small trees and understory grasses. Within each class, data at a higher resolution, 25 m, in subplots of 100 × 150 and 200 × 200 m were also collected (Fig. 1) The 25-m grid was accurately aligned with the 50 grid. The LAI of the sparse forest understory was not measured during this field campaign.

2.2. Instrumentation and data collection

Leaf area index (LAI), canopy and ground spectral reflectances were measured at this site during June 14th to 21st of 2000. LAI was measured with a LAI-2000 plant canopy analyzer (Li-Cor, Lincoln, Nebraska), which consists of a LAI-2070 control unit and a LAI-2050 sensor head. The sensor head projects the image of its nearly hemispheric view onto five detectors arranged in concentric rings (approximately 0–13°, 16–28°, 32–43°, 47–58°, 61–74°). A 270° view cap was used to eliminate the

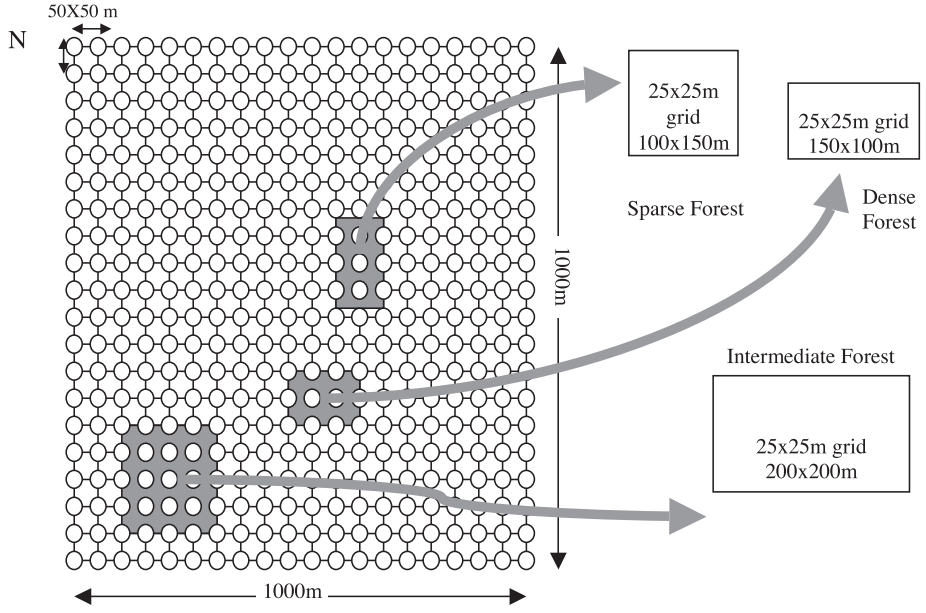

Fig. 1. Ruokolahti field campaign sampling strategy.

operator's shadow. Two LAI-2000 units were used to take simultaneous measurements within the forest and in an open area. They were inter-calibrated. The measurements were taken shortly before sunset, or during overcast days, when the forest was illuminated only by diffuse light. We followed the calibration procedure given in the LAI-2000 Plant Canopy Analyzer Instruction Manual, chapter 4-1 (LI-COR, 1992).

LAI values were calculated according to Miller's (1967) derivation, which is the default method used by LAI-2000. It should be noted, however, that the LAI-2000 converts canopy gap fraction into LAI under the assumption of uniformly distributed leaves (needles) and, moreover, the instrument cannot distinguish between foliage and woody material. Values from the Miller's formulae, therefore, give an effective leaf area index, L_e, which can be converted to the LAI as (Chen & Cihlar, 1996)

$$\mathrm{LAI} = (1-\alpha)L_e\gamma_e/\Omega_e, \quad (1)$$

where α is the woody-to-total area ratio, γ_e is the needle-to-shoot area ratio, and Ω_e is the element clumping index. In the MODIS LAI algorithm, a 1-year old shoot is taken as the basic foliage element (Knyazikhin et al., 1997; Tian et al., 2002a,b,c; Wang et al., 2003), uniformly distributed within the tree crown, and its projected silhouette area is taken as the foliage area, i.e., MODIS provides LAI values corresponding to Eq. (1) with $\gamma_e = 1$ and $\Omega_e = 1$. Values of the woody-to-total area ratio were set to 0.16. This value was obtained by averaging all values of α corresponding to needle forest sites reported by Chen and Cihlar (1996), as the required data for our site were not available.

GPS locations were made and differential correction performed within each grid level of the 1 × 1-km plot. Thus, a set of accurate geolocation measurements, with an uncertainty of about 2 m was obtained.

An ETM+ image collected on June 10, 2000 was used to generate a fine-resolution LAI map in our study. The image was atmospherically corrected using a simplified method for atmospheric correction (SMAC) algorithm (Rahman & Didieu, 1994). This technique is based on a set of semi-empirical equations with spectral band and sensor specific coefficients which are determined using a best-fit technique against the computations of the 6S radiative transfer code.

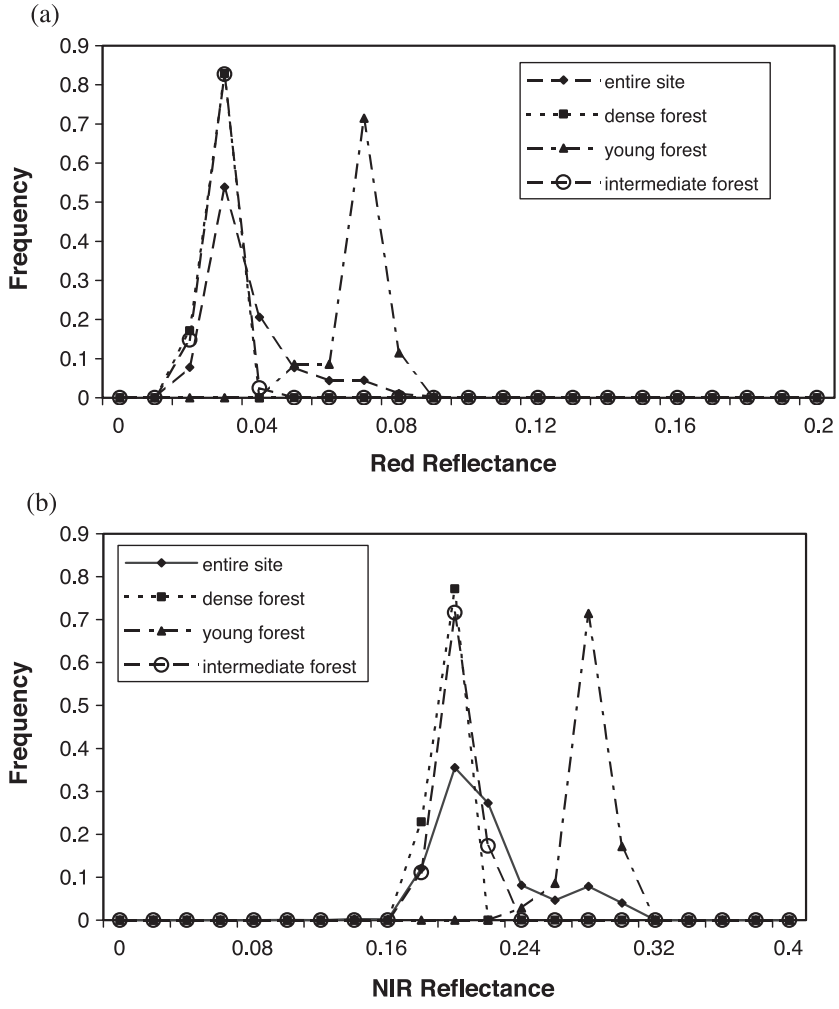

Fig. 2. Histograms of atmospherically corrected ETM+ reflectances at (a) red and (b) NIR spectral bands.

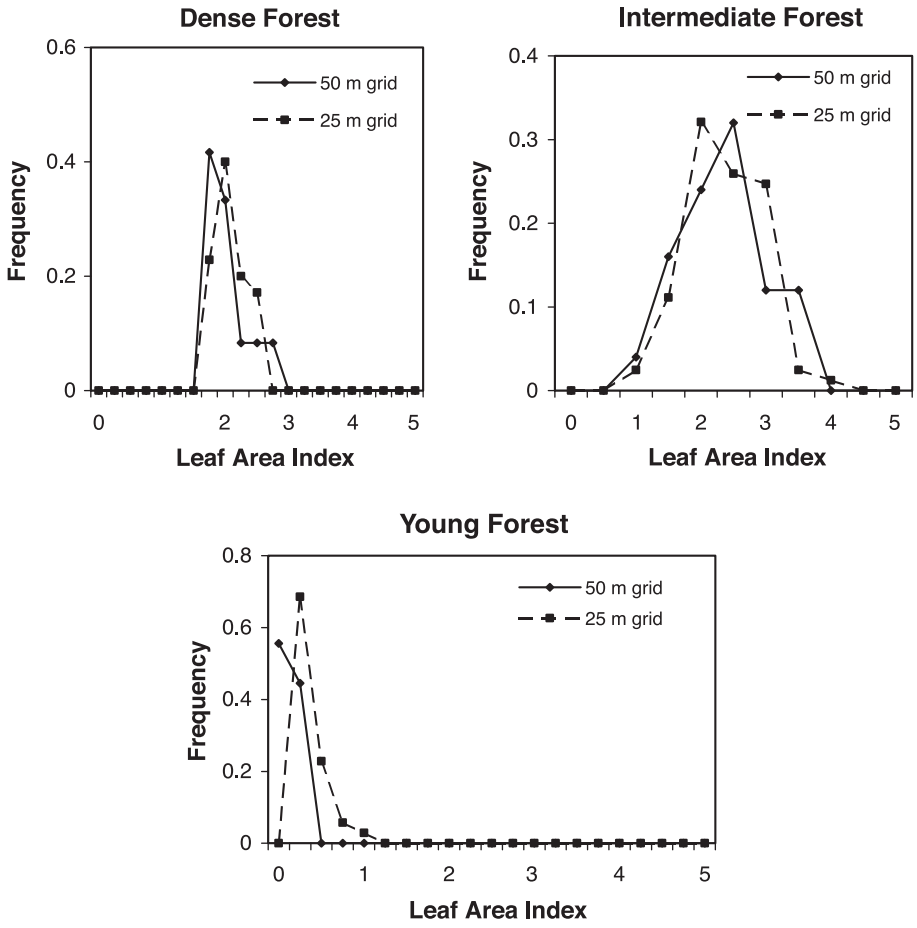

Fig. 3. Histograms of effective LAI values for sparse, intermediate and dense forests, at resolutions of 25 and 50 m.

Aerosol optical depth at 550 nm, input to the algorithm, was specified using technique reported in Häme et al. (2001). The ETM+ image was coregistered to the CCD image, hence coregistered to the ground.

3. Data analysis

Fig. 2 presents histograms of ETM+ red and near-infrared (NIR) reflectances of sparse, intermediate and dense forests sites. The sparse forest has distinct reflectance features compared to the others. The distributions of the ETM+ reflectances of the intermediate and dense forests are almost indistinguishable in these spectral bands. Typically, the reflectances of the intermediate and dense forests are about 0.023 in the red, and about 0.20 in the NIR bands. For the sparse forest, reflectances in these spectral bands are 0.07 and 0.27, respectively.

Fig. 3 presents histograms of effective LAI values for sparse, intermediate and dense forests collected at spacings of 25 and 50 m in the same subplots. Table 2 shows mean values of these histograms and their standard deviations. The

Table 1
Mean, standard deviation and *t*-test results of LAI for 50- and 25-m grid locations in the dense, sparse and intermediate forests

	Dense forest	Intermediate forest	Sparse forest
Mean (50 m)	1.91	2.06	0.07
S.D. (50 m)	0.36	0.68	0.11
Mean (25 m)	1.95	2.10	0.22
S.D. (25 m)	0.26	0.56	0.19
t-test (*P* value)	0.68	0.76	0.04

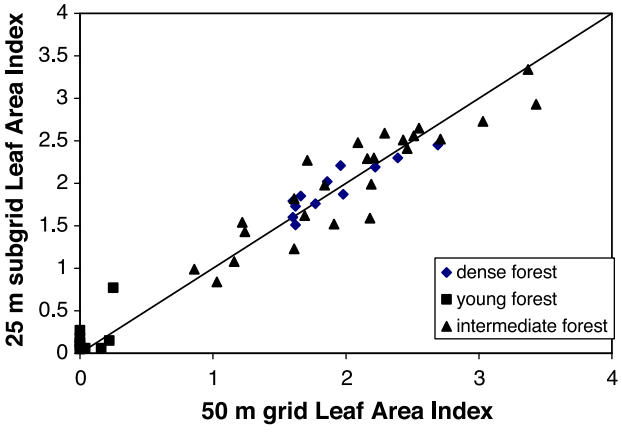

Fig. 4. Correlation between LAI measured at 50-m grid and corresponding 25-m subgrid.

mean effective LAI for the dense and intermediate forests are almost unchanged with sampling frequency. However, for the sparse forest, because the measuring height varied between the two measurements (25-m spacing measurement was performed at ground level while 50-m spacing measurement was performed at 1-m height), the mean values are substantially different. The *t*-test results show that the mean effective LAI values are not significantly different in the case of the dense and intermediate forests, while mean values for the sparse forest are not statistically equal (Table 1). Table 1 also shows that, generally, dense sampling results in lower variance, as would be expected.

In the three subplots, some grid points were measured twice because the subplots superimposed with the 50-m grid. These measurements were used to assess the uncertainty in the LAI measurements. Fig. 4 shows the correlation between LAI measured at 50-m grid and corresponding 25-m subgrid. The R^2 is 0.93 and RMSE is 0.23. This RMSE value indicates the uncertainty in the LAI measurements. It also sets a limit to the accuracy of LAI maps derived from these field measurements.

A contour plot of the effective LAIs is shown in Fig. 5a. One can see that the spatial distribution of the effective LAIs generally captures the spatial pattern of the 1×1-km site shown in the CCD picture (Fig. 5b); that is, low LAI values within the open area and high LAI values near the lower-left and lower-right corners, where the dense canopies are located.

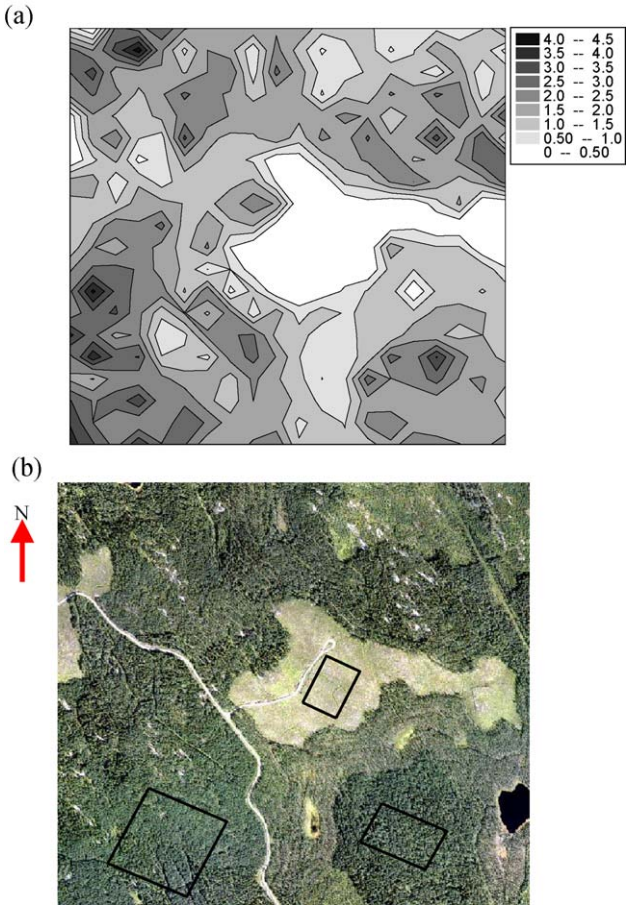

Fig. 5. (a) Contour plot of LAI values for the validation site and (b) its high-resolution CCD image.

4. Derivation of a fine-resolution LAI map

The biggest challenge for validation of moderate (100–1000 m) and coarse (> 1 km) resolution LAI products is the scarcity of ground-truth measurements. Considering the scale of in situ measurement (generally < 10 m per sample) and the large amount of work associated with field measurements, it is unrealistic to expect sufficient data for a pixel-by-pixel comparison. An alternative is to employ both field measurements and high-resolution satellite data to derive an accurate fine-resolution LAI map over a sufficiently extended area, degrade it to the coarse resolution, and compare this map with that derived from the coarse-resolution imagery. Thus, the first task is to derive a 30-m resolution LAI map of a 10×10-km region centered on the site where LAI measurements were made.

4.1. Adjustment of MODIS LAI algorithm at 30-m resolution

As a first attempt, the MODIS LAI algorithm was adjusted to 30-m resolution to produce a 30-m resolution LAI map of the validation site using the ETM+ reflectances. The algorithm requires a six-biome land cover classification (Myneni et al., 1997). All ETM+ pixels were treated as needle forests except for the sparse forest class. This class was mostly occupied by understory grasses and small shrubs and hence was treated as grasses.

The MODIS LAI algorithm uses a Look-Up Table (LUT) to retrieve LAI values. A three-dimensional radiative transfer equation is used to derive spectral and angular biome-specific reflectances of vegetation canopies. The numerical solutions of this equation are calculated and stored in the LUT. We begin with the Landsat TM LUT developed by Tian et al. (2002c) for the Northwest US (Washington and Oregon). The resulting correlation between retrieved LAI and field measured LAI at the pixel scale is shown in Fig. 6a. One can see that most of the retrieved LAIs are significantly greater than the field measured LAIs and their correlation is poor. Therefore, this LUT needed to be adjusted (Tian et al., 2002a,b,c).

Three factors influence the LAI retrieval of the MODIS LAI algorithm: (a) background reflectance which is an averaged effective reflectance of the surface underneath the canopy (soil or/and understory canopy); (b) canopy structure parameter which depends on the biome type and architecture of the vegetation canopy; (c) single-scattering albedo which is defined as the ratio of energy scattered by the elementary volume inside the canopy to the energy intercepted by this

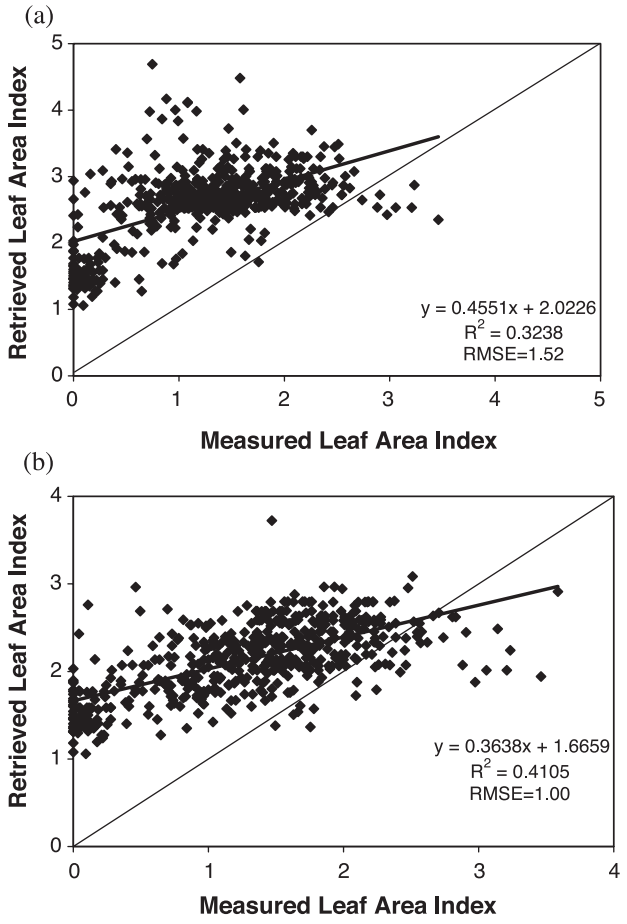

Fig. 6. Correlation between LAI retrieved by the MODIS LAI algorithm at 30-m resolution and field measured LAI at the pixel scale. (a) Before LUT adjustment; (b) after LUT adjustment.

volume. In the LUT of the algorithm, global vegetation was classified into six biome types using a vegetation cover classification parameterized in terms of variables used by photon transport theory (Myneni et al., 1997), each representing a pattern of the architecture of an individual tree (leaf normal orientation, stem–trunk–branch area fractions, leaf and crown size) and the entire canopy (trunk distribution, topography), as well as patterns of spectral reflectance and transmittance of vegetation elements. The soil and/or understory type are also characteristics of the biome, which can vary continuously within given biome-dependent ranges (Myneni et al., 1999). The single-scattering albedo describes the optical properties of elementary volume and varies significantly for different species in different parts in the world. A correct value of single-scattering albedo is required to obtain reliable retrieval.

The single-scattering albedo variable is assumed biome-specific constant with respect to spatial and directional variables in the algorithm. However, it also depends on the definition of the scattering center and the size of elementary volume considered in the formulation of the radiative transfer equation. Since the canopy architecture also depends on the definition of the scattering center, the canopy structure parameter also depends on it. Therefore, the canopy structure parameter must be consistent with the single-scattering albedo. For example, if a cube of $50 \times 50 \times 50$ cm is taken as an elementary volume in a coniferous forest, a 1-year shoot of 5–7 cm should be taken as a scattering center (Knyazikhin et al., 1997). The single-scattering albedo, in this case, characterizes scattering properties of the $50 \times 50 \times 50$-cm cube filled with 1-year shoots, and all coefficients of the transport equation should be derived for such $50 \times 50 \times 50$ cells.

LAI is nonlinearly related to single-scattering albedo and canopy structure parameter, nevertheless, changing the single-scattering albedo will change the distribution of retrieved LAI. The LUT can be adjusted by tuning the single-scattering albedo or canopy structure parameter to find the best match between algorithm-retrieved LAI and field-measured LAI. The LUT was adjusted through matching the distributions of retrieved LAI and field measured LAI. Fig. 6b shows the results after tuning the single-scattering albedo, which improves the overall relationship, but the results appear noisy. The reason for this is carefully analyzed in the following section.

4.2. Validation of MODIS LAI algorithm at 30-m resolution

Although every effort has been made to obtain accurate geolocation of each sampling point and ETM+ pixels, this still does not guarantee that the sampling point falls within the specified satellite pixel. An illustration of pixel-by-pixel comparison is shown in Fig. 7a. Field samples often fall on the boundary or out of the pixel. Moreover, one or even a few measurements in a single pixel may be insufficient to represent the pixel mean value because the area measured with the LAI-2000 is considerably smaller than ETM+ pixels. The LAI values in this forest area exhibit high variance over short distances, as first noted by Tian et al. (2002a). Based on a hierarchical decomposition of variograms (Collins & Woodcock, 2000; Woodcock et al., 1997), Tian et al. (2002b) proposed a patch-based comparison method to scale field measurements to the spatial scale of satellite observations.

For the analysis of remotely sensed imagery, a landscape can be regarded as a collection of smaller objects, such as forest stands or other homogenous patches of vegetation. In essence, the landscape may be assumed to be composed of a set of objects which are more homogenous within than between them (Collins & Woodcock, 2000). In this situation, satellite pixels are assumed to be samples of objects. When pixels are small relative to objects, internal variance of the objects can adversely affect the analysis (Markham & Townshend, 1981). On the other hand, when the pixel size is large relative to the objects, an individual pixel often covers parts of two or more objects, resulting in mixed pixels, and the effectiveness of analysis is undermined (MacDonald & Hall, 1980). An ideal condition would result when remote measurements correspond directly to the objects in the scene

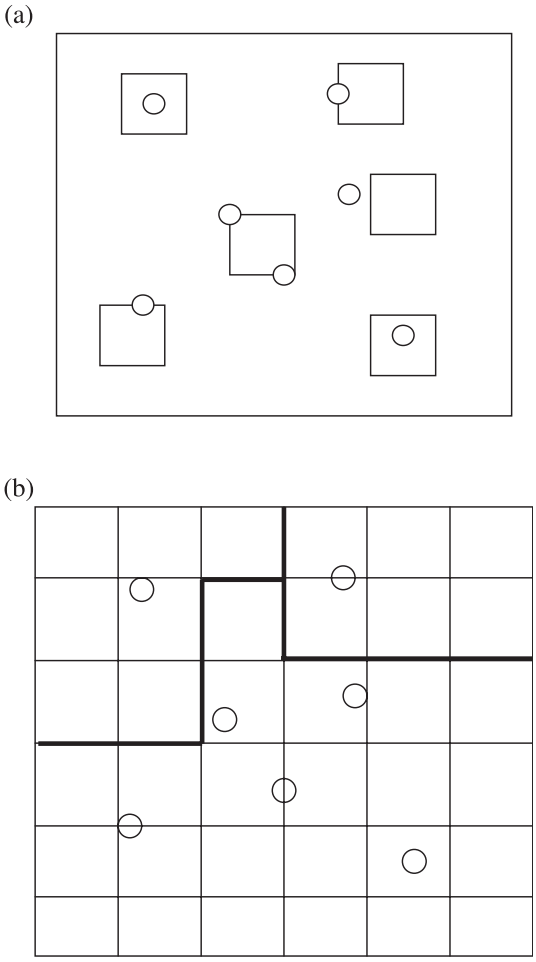

Fig. 7. The schemes of comparison between satellite pixels and field samples. (a) Pixel-by-pixel comparison; (b) patch-by-patch comparison. Circles represent field samples and squares represent satellite pixels.

(Woodcock & Harward, 1992), a situation which is not observed in nature due to the variance in object size.

One way to try to minimize the effects of sparse sampling of ETM+ pixels and possible geolocation errors is to shift the scale of analysis from pixels to forest stands, or patches. The patches should satisfy the following conditions: (a) their internal variance is small such that a patch can be regarded as a relatively homogenous area and a small amount of sampling is sufficient to characterize the mean feature of the object; (b) each patch should be large enough such that effect of geolocation errors is minimized. In this case, each point measurement can be regarded as a random sample of a larger area. This increases the probability that the sampling point falls inside the patch, with the mean value of these samples serving as an estimate of the true mean of the entire patch. Fig. 7b shows the scheme of a patch-by-patch comparison. Without extraordinary registration accuracy and high-sampling density, a patch-by-patch comparison is more reliable than a pixel-by-pixel comparison.

Image segmentation can be used to generate patches in images. The objective of image segmentation is to partition the image into a set of patches, which correspond to objects on the ground (Beaulieu & Goldberg, 1989). It groups pixels into patches based on their spectral similarity and adjacency. The decision of the size and number of patches are based on following considerations: (a) patches cannot be too small, which ensures enough field samples in each patch and reduce geolocation errors; (b) patches cannot be too big, which ensures enough number of patches for statistics and also preserves patch homogeneity. Using this method, the 1-km ETM+ image of the validation site was divided into 19 patches. Each consists of tens to hundreds of pixels and is relatively homogenous (Fig. 8). All seven available ETM+ spectral bands were used in the segmentation procedure. Table 2 shows the mean values of red and NIR reflectances over these segments and their standard deviations. The coefficient of variation does not exceed 10^{-2} indicating that the segments can be treated as homogeneous areas with respect to their red and NIR reflectances. However, the LAI values exhibit higher variation within the patches (Table 3). If the coefficient of variation is taken as a measure of uncertainty, most of the patches can be represented by the mean LAI value within

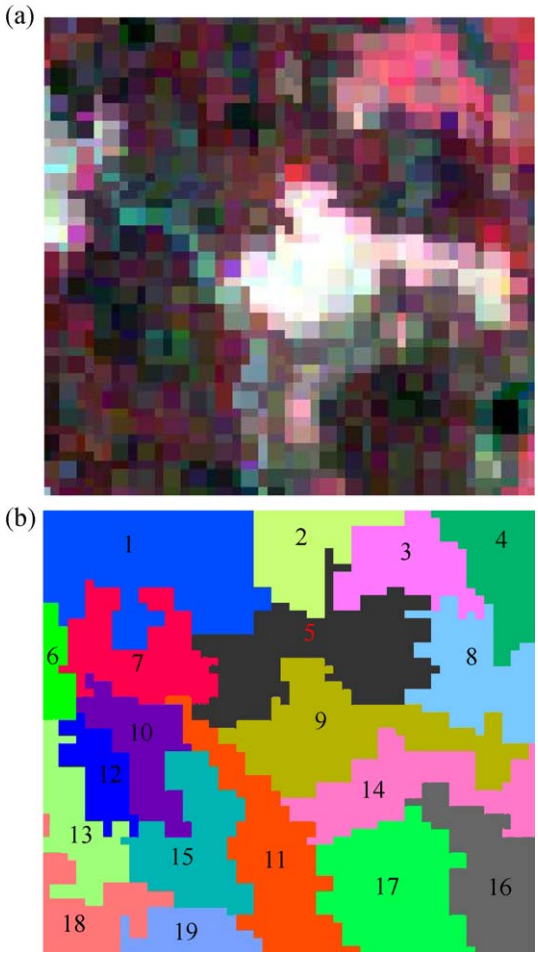

Fig. 8. (a) RGB image of the 1-km region of Ruokolahti from ETM+ bands 4, 3, 2. (b) Map of the 1-km region using a segmentation procedure.

Table 2
Mean ETM+ reflectances over patches, their standard deviations and number of pixels per segment

Patch no.	Red band		NIR band		Number of pixels
	Mean	S.D.	Mean	S.D.	
1	0.02311	1.21e − 05	0.1883	0.0003	218
2	0.02685	3.25e − 05	0.2014	0.000172	67
3	0.03778	2.98e − 05	0.2561	0.000235	79
4	0.03489	3.60e − 05	0.2378	0.00032	38
5	0.02895	2.96e − 05	0.2087	0.00036	286
7	0.03185	6.05e − 05	0.1933	0.000362	149
8	0.02445	3.66e − 05	0.2021	0.000359	121
9	0.06119	9.27e − 05	0.274	0.000253	244
10	0.02503	1.78e − 05	0.1849	8.31e − 05	121
11	0.03958	65e − 05	0.2205	0.000373	175
12	0.02176	5.18e − 06	0.1766	6.05e − 05	74
13	0.0242	1.04e − 05	0.1991	5.56e − 05	91
14	0.03611	3.30e − 05	0.2145	0.0002	149
15	0.02527	1.07e − 05	0.1979	7.81e − 05	174
16	0.02773	1.33e − 05	0.1968	65e − 05	44
17	0.02366	1.16e − 05	0.185	6.07e − 05	202
18	0.02365	1.22e − 05	0.185	5.41e − 05	26

an uncertainty of 20%. However, in some segments (1, 4, 8 and 9) the uncertainty can be high.

The patch map shown in Fig. 8 was then used to produce mean LAIs over each patch. Fig. 9 demonstrates a patch-by-patch correlation between measured and retrieved LAI values. Although the correlation between retrieved LAI and field measured LAI is improved after adjustment of the LUT, significant disagreement still exists. The disagreement between the measured and retrieved LAI values is a decreasing function of LAI. One possibility is the effect of understory vegetation, as the field measurements do not capture the effect of the understory. Thus, the field measurements only characterize the forest canopy yet the reflectance in the imagery includes the understory, which includes

Table 3
Mean Leaf Area Index (LAI) of segments, standard deviations, coefficients of variation, and number of samples in the segment

Patch no.	Mean LAI	S.D.	S.D./Mean	Number of samples
1	2.035	0.5514	0.270958	42
2	1.631	0.2743	0.168179	14
3	1.02	0.1721	0.168725	16
4	1.322	0.586	0.443268	10
5	1.562	0.2486	0.159155	43
7	1.259	0.4844	0.38475	26
8	1.897	0.6777	0.357248	22
9	0.2258	0.2106	0.932684	38
10	1.509	0.3049	0.202054	16
11	1.105	0.2236	0.202353	30
12	2.606	0.3465	0.132962	13
13	2.623	0.3557	0.135608	17
14	0.895	0.1727	0.192961	28
15	1.924	0.327	0.169958	31
16	1.423	0.02948	0.020717	10
17	1.986	0.2177	0.109617	34
18	2.712	0.5147	0.189786	8

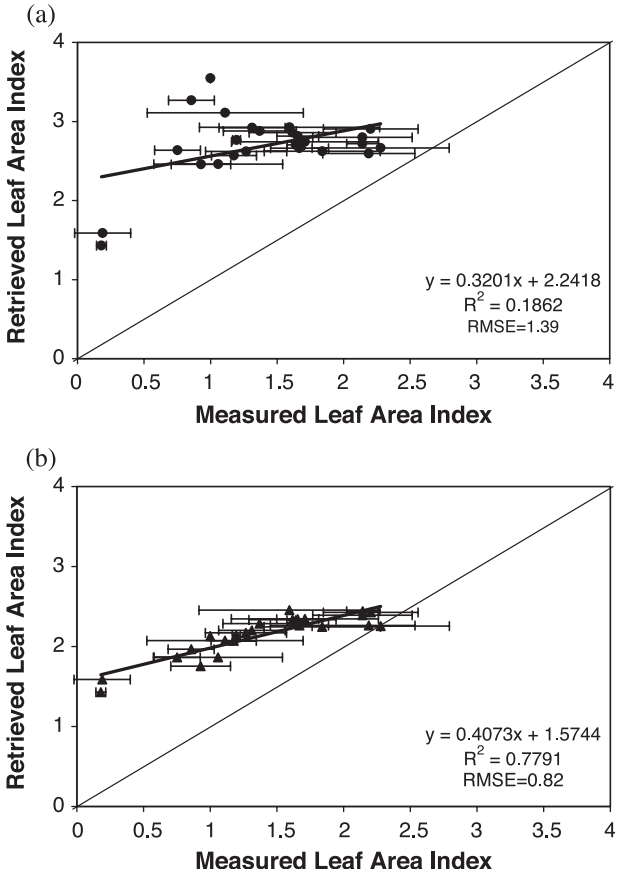

Fig. 9. Correlation between LAI retrieved by the MODIS LAI and FPAR algorithm at 30-m resolution and field measured LAI at patch scale: (a) before LUT adjustment; (b) after LUT adjustment.

mosses, shrubs and small trees. In this situation, one would expect estimates of LAI from imagery to exceed those measured on the ground and the effect to be larger at low canopy LAI values as the understory is more visible from above, as is observed in Fig. 9b.

4.3. Generating a fine-resolution LAI map of the 1×1-km using empirical approaches

In hopes of producing a better high-resolution LAI map for comparison with MODIS retrievals, empirical methods were tested. Numerous similar studies have been performed to relate ground-measured LAI to satellite observations (Chen & Cihlar, 1996; Fassnacht et al., 1997; Franklin, 1986; Nemani et al., 1993; Spanner et al., 1990; Tian et al., 2002a,b). A widely used approach is to regress ground-measured LAI on vegetation indices such as the normalized differential vegetation index (NDVI) and the simple ratio (SR). The NDVI is the most commonly used vegetation index for LAI retrievals. This variable is defined in terms of red and NIR reflectances, ρ_{red} and ρ_{NIR},

$$\mathrm{NDVI} = \frac{\rho_{NIR} - \rho_{red}}{\rho_{NIR} + \rho_{red}}. \quad (2)$$

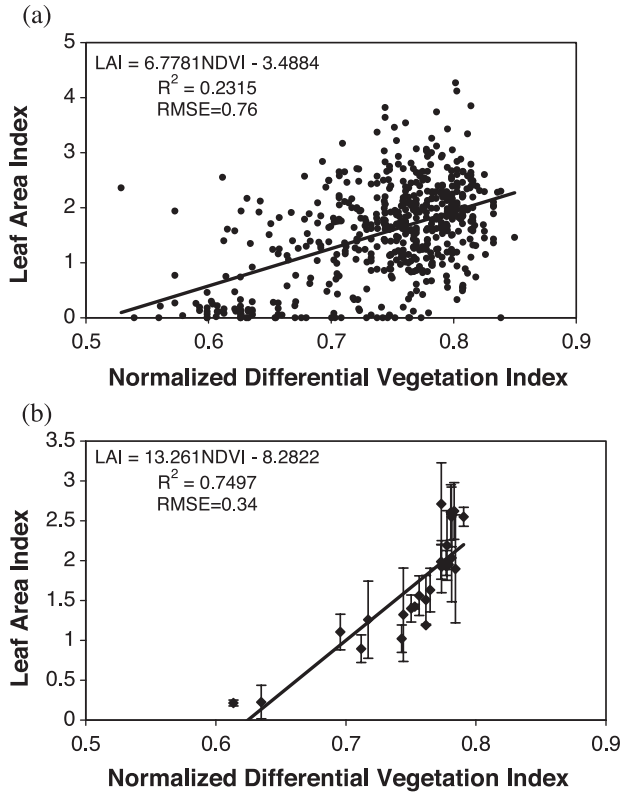

Fig. 10. Correlation between the normalized differential vegetation index (NDVI) and field measured LAI at (a) pixel comparison and (b) patch scale.

Fig. 10a shows that the pixel-by-pixel correlation between field-measured LAI and satellite-derived NDVI is low; the R^2 is 0.23 in this case. These results appear noisy in much the same fashion as previous results based on pixels (Fig. 6). As Tables 3 and 4 indicate, LAI values can vary considerably with reflectances in red and NIR spectral bands essentially unchanged. This results in poor correlation between the field-measured LAI and satellite-derived NDVI.

The correlation improves considerably if patches are used as the element of the analysis. The correlation between mean NDVI and mean field-measured LAI of patches is shown in Fig. 10b. The R^2 increases to 0.73 with a RMSE of 0.34. Note that mean reflectances of the patches were used in Eq. (2) to calculate the mean NDVI.

Although a good correlation can be obtained at the patch scale between NDVI and LAI, the dynamic range in NDVI is small. Fig. 10b shows that mean NDVI values fall in the interval between 0.6 and 0.8, while the LAI values vary between 0.2 and 2.7.

The simple ratio (SR) is another index used to relate LAI values to satellite data. For a given area, this variable is the ratio of NIR to red reflectance. Fig. 11 shows the pixel and patch level relationship between the SR and LAI. Again, the pixel level relationship is poor between field measured LAI and the SR ($R^2 = 0.20$). However, at the patch level, a better relationship is obtained ($R^2 = 0.82$, RMSE = 0.29). The range of the SR is between 4.5 and 9.0. It should be noted that there is a direct but nonlinear relationship between the SR and NDVI; that is, SR=(1 + NDVI)/(1 − NDVI), and thus SR and NDVI contain similar information.

The understory strongly affects the SR and NDVI. The influence of the understory on these variables can be quite high, as our field LAI measurements were taken for overstory canopy only. The understory NDVI can be as high as 0.6. The contribution of understory to NDVI or SR is also a function of canopy closure (Franklin, 1986; Spanner et al., 1990). Several studies suggest that the use of shortwave infrared (SWIR) reflectances can account for the background reflectances (Baret et al., 1988; Brown et al., 2000; Butera, 1986; Nemani et al., 1993). A modified form of the simple ratio, or the reduced simple ratio (RSR) was proposed by Brown et al. (2000):

$$\mathrm{RSR} = \frac{\rho_{\mathrm{NIR}}}{\rho_{\mathrm{red}}}\left[1 - \frac{\rho_{\mathrm{SWIR}} - \min(\rho_{\mathrm{SWIR}})}{\max(\rho_{\mathrm{SWIR}}) - \min(\rho_{\mathrm{SWIR}})}\right] \quad (3)$$

where ρ_{SWIR} is the shortwave infrared reflectance, which can be obtained from Band 5 of ETM+ data, and the $\min(\rho_{\mathrm{SWIR}})$ and $\max(\rho_{\mathrm{SWIR}})$ are the minimum and maxi-

Table 4
Regression models reported in literature to relate Leaf Area Index (LAI) and vegetation indices derived from Landsat TM data

Vegetation Index	Field LAI measurements	Equation	R^2	Author
NDVI/SR	Allometric method	$\mathrm{LAI} = 0.5724 + 0.0989\mathrm{LAI} - 0.0114\mathrm{LAI}^2 + 0.0004\mathrm{LAI}^3$	0.74	Turner et al. (1999)
		$\mathrm{SR} = 2.2282 + 2.5376\mathrm{LAI} - 0.1576\mathrm{LAI}^2$	0.59	
NDVI/SR	Allometric method	$\mathrm{NDVI} = 0.0377\mathrm{LAI} + 0.607$	0.72	Fassnacht et al. (1997)
		$\mathrm{SR} = 0.9357\mathrm{LAI} + 3.552$	0.71	
SR	Allometric method	$\mathrm{SR} = 1.92\mathrm{LAI}^{0.583}$	0.91	Peterson et al. (1987)
		$\mathrm{SR} = 1.92 + 0.532\mathrm{LAI}$	0.83	
NDVI/SR	LAI-2000 and TRAC*	$\mathrm{NDVI} = 0.032\mathrm{LAI} + 0.635$	0.42	Chen and Cihlar (1996)
		$\mathrm{SR} = 1.014\mathrm{LAI} + 3.637$	0.49	
SR	LAI-2000 and TRAC*	$\mathrm{SR} = 1.153\mathrm{LAI} + 2.56$	0.66	Chen et al. (2002)
SR	Ceptometer	$\mathrm{SR} = 3.1196 + 5857\log(\mathrm{LAI})$	0.97	Spanner et al. (1994)
NDVI/SR	LAI-2000	$\mathrm{NDVI} = 1.2383/(1/\mathrm{LAI} + 0.9061) - 0.3348$	0.87	Gong et al. (1995)
		$\mathrm{SR} = 0.96/(1/\mathrm{LAI} - 0.066) + 0.987$	0.88	
NDVI	Allometric method	$\mathrm{LAI} = 33.99\mathrm{NDVI} - 121$	0.75	Curran et al. (1992)
SR	Allometric method	$\mathrm{SR} = 0.614\mathrm{LAI} + 1.23$	0.82	Running et al. (1986)
NDVI	Allometric method	$\mathrm{NDVI} = 0.03\mathrm{LAI} + 0.6$	0.32	Nemani et al. (1993)

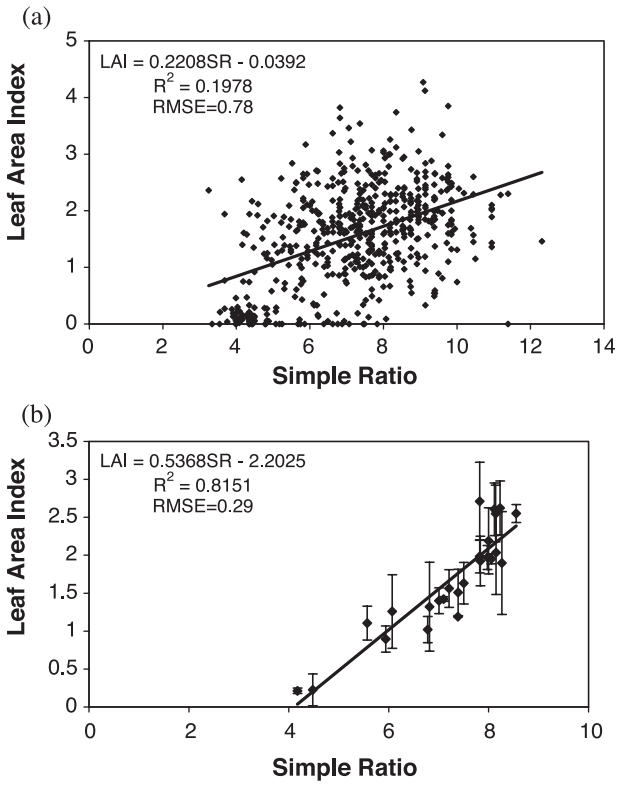

Fig. 11. Correlation between simple ratio (SR) and field-measured LAI at (a) pixel and (b) patch scale.

mum SWIR reflectance found in the ETM+ image. The advantages of RSR over SR are (Brown et al., 2000; Chen et al., 2002): (a) the background influence is suppressed because the SWIR band is mainly sensitive to the amount of vegetation containing liquid water in the background; and (b) the difference between cover types is reduced, so a single LAI algorithm can be developed without using a coregistered landcover map.

Fig. 12 shows the relationship between RSR and LAI at the patch scale ($R^2 = 0.91$; RMSE = 0.22). Note that the mean reflectance over the corresponding patch was used in Eq. (3) to calculate the patch RSR. The linear regression is

$$\mathrm{LAI} = 0.4693\mathrm{RSR} - 0.6277 \quad (4)$$

This relationship was applied to a 10 × 10-km ETM+ scene centered on the validation site to generate a fine-resolution LAI map. This 10-km area was first segmented into patches and then Eq. (4) was applied to each patch. Fig. 13 shows LAI maps of the 10-km area and its central part, the 1-km area, derived from the ETM+ image using relationship (4). The LAI map of the 1 × 1-km captures the basic spatial features shown in Fig. 5b, namely, the sparse forest in the middle of the image, and the dense forest on the lower-left and lower-right corners.

The RMSE for relationship (4) is 0.22, which is taken as a measure of the uncertainty. Assuming that relationship (4)

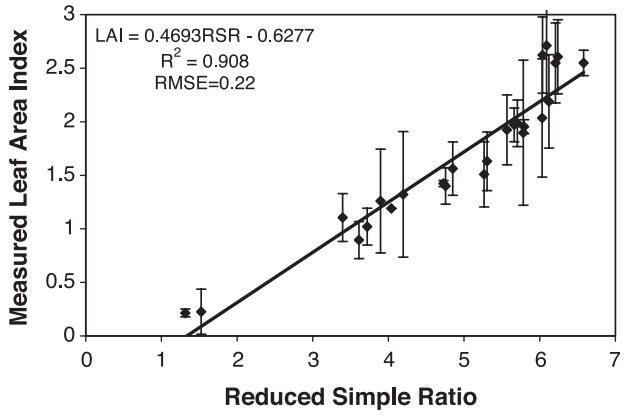

Fig. 12. Patch level comparison between Leaf Area Index (LAI) and reduced simple ratio (RSR).

is valid for the entire 10 × 10-km area, and assuming that uncertainties in the channel ETM+ data do not affect the reduced simple ratios (Eq. (3)), one can conclude that the

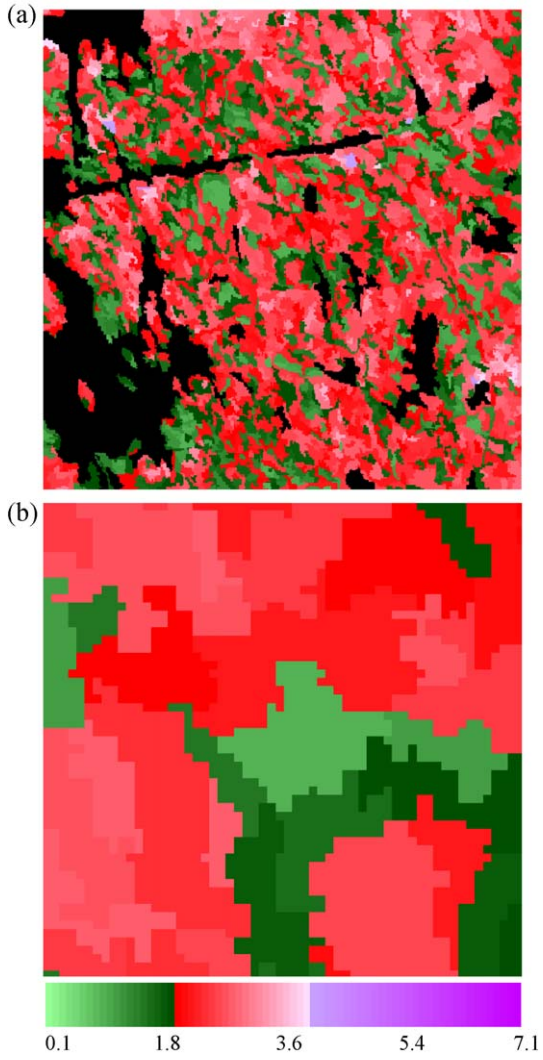

Fig. 13. (a) 10 × 10-km LAI maps derived from the ETM+ image using relationship (4) and (b) its 1 × 1-km central part.

uncertainty of the fine resolution LAI map is 0.22. This is consistent with the estimation in Fig. 4 (RMSE = 0.23).

5. Validation of the MODIS LAI product

5.1. The MODIS LAI product

The MODIS LAI product is produced at 1-km spatial resolution daily (MOD15A1) and composited over an 8-day period based on the maximum FPAR value. The 8-day product (MOD15A2) is distributed to the public from the EROS Data Center Distributed Active Archive Center (EDC DAAC). Its accuracy is expected to be 0.5 LAI. The products are projected on the Integerized Sinusoidal (IS) 10° grid, where the globe is divided for production and distribution purposes into 36 tiles along the east–west axis, and 18 tiles along the north–south axis, each approximately 1200 × 1200 km. Each tile contains LAI, FPAR and two quality assessment (QA) variable data sets (Myneni et al., 2002). The QA variable data sets contain information about retrieval status such as the overall quality of input data, cloud condition, algorithm used to retrieve LAI. The MODIS LAI algorithm uses a biome classification map and atmospherically corrected MODIS spectral reflectances at 1-km resolution to retrieve LAI. It compares measured reflectances with those determined from a suite of canopy models, which depend on biome type, canopy structure, and soil/understory reflectances. The canopy/soil/understory models for which simulated and measured surface reflectances do not exceed uncertainties in model and observations are used to derive the distribution of all possible solutions, i.e., LAI distribution functions. The mean values of these distribution functions are archived. The overall uncertainty (Wang et al., 2001) in model and observations is set to 20% which are lower than actual uncertainties in MODIS surface reflectance at red and near-infrared spectral bands (Huang et al., 2004). Should this main algorithm fail, a backup algorithm is triggered to estimate LAI using vegetation indices. Information on which algorithm was used is archived in the QA variable data set. In the case of a dense canopy, its reflectance can be insensitive to various parameters (e.g., LAI) characterizing the canopy. When this happens, the canopy reflectance is said to belong to the saturation domain (Knyazikhin et al., 1998b). This situation is recognized by the retrieval technique (Knyazikhin et al., 1998b) and reported in the QA variables. It also should be noted that the MODIS algorithm is executed independently of information provided by the cloud mask. Therefore, users are required to consult the QA file to select LAI values retrieved under clear sky conditions.

5.2. Validation of the MODIS LAI product

The Collection 4 MOD15A2 products for June 2000 (days 153–160, 161–168, 169–177 and 178–184, a period from June 1 to July 1, 2000) were used in our analysis. The Ruokolahti Forest is located in the tile h19v02, line 1016 and sample 442. The 30-m resolution map derived using the regression based on RSR was first coregistered to MODIS projection and then degraded to 1-km resolution by averaging all fine resolution LAI values within each MODIS pixel. In the aggregation procedure, LAI of water and barren pixels were set to zero. A 5 × 5-km region centered on the validation site was extracted from both the corresponding MODIS tiles and coregistered ETM+ scene. MODIS LAI values produced by the main algorithm without saturation under clear sky conditions were selected. To maximize number of pixels satisfying these conditions, MODIS LAIs from all four tiles were used to generate one 5 × 5-km map of mean LAI. The MODIS algorithm is designed to retrieve a distribution function of all possible LAI values of a pixel on the basis of the spectral information and biome type, taking the mean of the distribution function as the retrieved LAI (Knyazikhin et al., 1998b; Tian et al., 2000; Wang et al., 2001). Theoretically, it is possible that the LAI of a single MODIS pixel is not retrieved accurately due to uncertainties in inputs and the algorithm, but the mean of multiple retrievals over a region with similar pixels is accurately retrieved. In the validation of MODIS LAI product, therefore, it is not appropriate to make pixel-by-pixel comparison as this can result in a poor correlation (Fig. 14). It is essential to perform comparisons at multi-pixel-patch scale to account for uncertainties in the product arising from uncertainties in inputs to the LAI-FPAR algorithm. We divided the aggregated ETM+ LAI map into several patches according to the similarity of LAI values such that each patch can be represented by the mean ETM+ LAI value sufficiently well. Mean MODIS LAI values over these patches were also calculated. Fig. 15 shows the patch-by-patch relationship between the MODIS and aggregated LAI values. One can see that a better agreement is achieved at the patch scale. However,

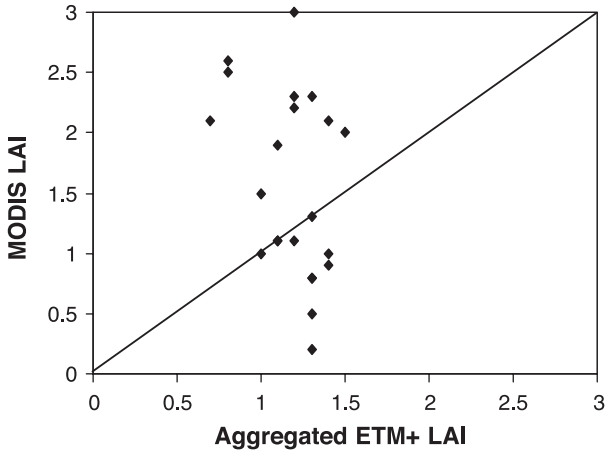

Fig. 14. Pixel-by-pixel correlation between the MODIS and aggregated ETM+ Leaf Area Index (LAI) values.

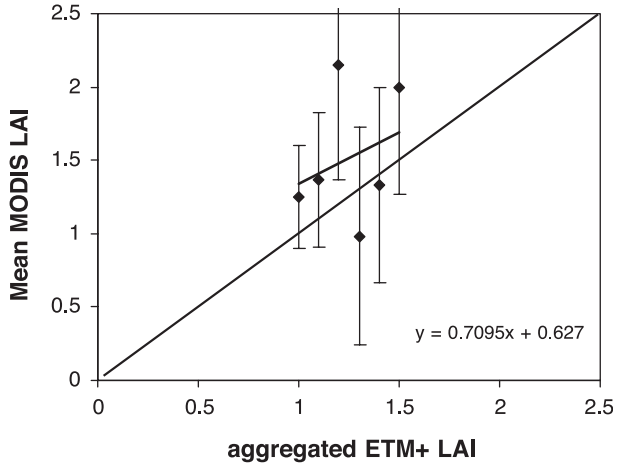

Fig. 15. Patch-by-patch relationship between the MODIS and aggregated ETM+ Leaf Area Index (LAI) values.

the mean variance is 48% which is higher than an overall uncertainty of 20% used by the operational MODIS LAI algorithm. This discrepancy can be due both deficiencies in physics of the LAI algorithm and uncertainties in atmospherically surface reflectance. These two factors can result in the actual overall uncertainty to be exceeded a tolerance level of 20% currently used by the algorithm. With the exception of one retrieved value, the MODIS LAIs are within an accuracy of 0.5 LAI and thus meet accuracy requirements for the LAI product.

6. Discussion and conclusions

The analysis presented suggests that the pixel-by-pixel correlation between field-measured LAI and vegetation indices can be very low. Patch level comparisons improve the correlation between field measurements and satellite derived vegetation indices because this reduces the registration errors and the averaged field measurements are more representative of the mean LAI of the whole patch.

For a specific site, empirical approaches work well to produce a fine resolution LAI map from satellite data because the regression processes finds the best fit between field measurements and satellite data and eliminates the problem of systematic bias. Various relationships such as linear (Chen & Cihlar, 1996; Chen et al., 2002; Curran et al., 1992; Fassnacht et al., 1997; Nemani et al., 1993; Peterson et al., 1987; Running et al., 1986), polynomial (Turner et al., 1999), power (Peterson et al., 1987), logarithm (Spanner et al., 1994) and other (Gong et al., 1995) regressions have been used to estimate LAI from TM images. Table 4 lists the regression models reported in literature that relate field LAI measurements and these vegetation indices derived from Landsat TM data for coniferous forests with R^2 values ranging from 0.32 to 0.97. These relationships are also influenced by the difference in LAI definition, field measurement method and atmospheric correction of the satellite image (Running et al., 1986). Fig. 16 plots these regression curves. One can see that the regression models are highly site-specific; there is no uniform relationship between vegetation indices and field measured LAI for all those sites, especially when the canopy is dense (high LAI) because the surface reflectance is insensitive to LAI change in this case. Therefore, although very good correlation between satellite-derived vegetation indices and field measured LAI can be achieved for a specific site, empirical methods do not consider the physics behind the regression relationships and are highly site dependent, and thus cannot be generalized to very large areas or different sites, their utility is limited.

A patch-level comparison of the aggregated high-resolution LAI map with corresponding MODIS LAI retrievals reveals good correspondence between the two and imbues confidence in the MODIS LAI algorithm although variation in LAI retrievals are higher than expected. We failed to adjust the LAI algorithm to produce a fine-resolution LAI map for this particular site. The ETM+ pixels coincide with the finest resolution that the algorithm can recognize and which is assumed to represent one pure biome type in each pixel. In the case of the Ruokolahti site, a forest biome can be mixed with understory sprigs, shrubs, mosses and grasses within the 30-m pixel, causing high uncertainties in the specification of biome type which is input to the algorithm. The creation of a Look-up-Table (LUT) finer than 30-m resolution is a possible solution to account for biome mixture at 30-m resolution. Alternatively, radiative transfer models for multiple layer vegetation canopies which count in understory vegetation effect could be explored.

The single-scattering albedo is a very important variable for LAI retrieval when using a radiative transfer based method. It depends on the size of the elementary volume and optical properties of scattering centers, although it is not clear as how to measure the mean single-scattering albedo systematically over a site or how to account for the influence

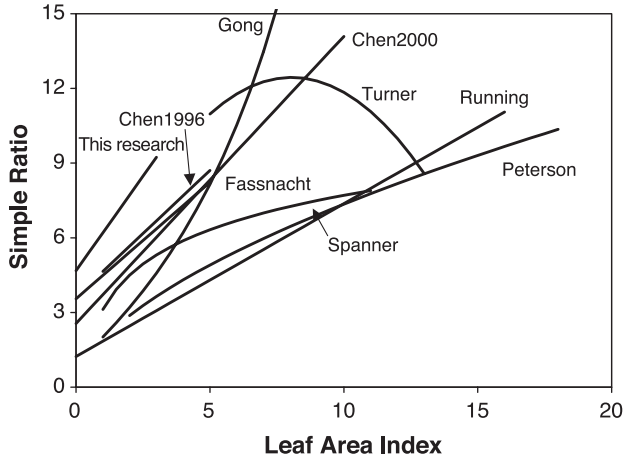

Fig. 16. Regression curves between simple ratio (SR) and LAI reported in literature.

of understory vegetation and how it changes with scale. The single-scattering albedo of an elementary volume could be retrieved using hyperspectral canopy reflectance and transmittance data (Wang et al., 2003). An alternate way could be calculating from a shoot model according to the optical properties of a single needle.

This analysis also indicated that the reduced simple ratio (RSR), which includes red, near-infrared and shortwave infrared bands, is best correlated with field LAI measurements. Thus, it appears that the use of shortwave infrared band in MODIS LAI retrievals over needle leaf forests should be investigated.

References

Baret, F., Guyot, G., Begue, A., Maurel, P., & Podaire, A. (1988). Complementarity of middle infrared with visible and near-infrared reflectance of monitoring wheat canopies. *Remote Sensing of Environment*, *26*, 213–225.

Beaulieu, J. M., & Goldberg, M. (1989). Hierarchy in picture segmentation: A stepwise optimization approach. *IEEE Transactions on Pattern Analysis and Machine Intelligence*, *11*, 150–163.

Bonan, G. B. (1996). A Land Surface Model (LSM version 1.0) for ecological, hydrological, and atmospheric studies: *Technical Description and user's guide, NCAR/TN-417+STR* (pp. 88–102).

Brown, L., Chen, J. M., Leblanc, S. G., & Cihlar, J. (2000). A shortwave infrared modification to the simple ratio for LAI retrieval in Boreal forests: An image and model analysis. *Remote Sensing of Environment 71*, 16–25.

Butera, C. (1986). A correlation and regression analysis of percent canopy closure and TM spectral response for selected forest sites in San Juan national forest Colorado. *IEEE Transactions on Geoscience and Remote Sensing*, *24*, 122–129.

Chen, J. M., & Black, T. A. (1992). Defining leaf area index for non-flat leaves. *Plant, Cell and Environment*, *15*, 421–429.

Chen, J. M., & Cihlar, J. (1996). Retrieving leaf area index of boreal conifer forests using Landsat TM images. *Remote Sensing of Environment*, *55*, 153–162.

Chen, J. M., Pavlic, G., Brown, L., Cihlar, J., Leblanc, S. G., White, H. P., Hall, R. J., Peddle, D. R., King, D. J., Trofymow, J. A., Swift, E., Van der Sanden, J., & Pellikka, P. K. E. (2002). Derivation and validation of Canada-wide coarse-resolution leaf area index maps using high-resolution satellite imagery and ground measurements. *Remote Sensing of Environment*, *80*, 165–184.

Cohen, W. B., Maiersperger, T. K., Yang, Z., Gower, S. T., Turner, D. P., Ritts, W. D., Berterretche, M., & Running, W. (2003). Comparison of land cover and LAI estimates derived from ETM+ and MODIS for four sites in North America: A quality assessment of 2000/2001 provisional MODIS products. *Remote Sensing of Environment*, *88*, 233–255.

Collins, J. B., & Woodcock, C. E. (2000). Combining geostatistical methods and hierarchical scene models for analysis of multiscale variation in spatial data. *Geographical Analysis*, *32*(1), 50–63.

Curran, P. J., Dungan, J. L., & Gholz, H. L. (1992). Seasonal LAI in slash pine estimated with Landsat TM. *Remote Sensing of Environment*, *39*, 3–13.

Dickinson, R. E., Henderson-sellers, A., Kennedy, P. J., & Wilson, M. F. (1986). Biosphere–atmosphere transfer scheme (BATS) for the NCAR Community Climate Model. *Tech. Note TN-275+STR*. National Center for Atmospheric Research, Colorado (pp. 72).

Fassnacht, K. S., Gower, S. T., MacKenzie, M. D., Nordheim, E. V., & Lillesand, T. M. (1997). Estimating the leaf area index of north central Wisconsin forest using the Landsat Thematic Mapper. *Remote Sensing of Environment*, *61*, 229–245.

Foley, J. A., Levis, S., Prentice, I. C., Pollard, D., & Thompson, S. L. (1998). Coupling dynamic models of climate and vegetation. *Global Change Biology*, *4*, 561–579.

Franklin, J. (1986). Thematic mapper analysis of coniferous forest structure and composition. *International Journal of Remote Sensing*, *10*, 1287–1301.

Gong, P., Pu, R., & Miller, J. R. (1995). Coniferous forest leaf area index estimation along the Oregon Transect using Compact Airborne Spectrographic Imager data. *PE & RS*, *61*, 1107–1117.

Häme, T., Stenberg, P., Andersson, K., Rauste, Y., Kennedy, P., Folving, S., & Sarkeala, J. (2001). AVHRR-based forest proportion map of the Pan-European area. *Remote Sensing of Environment*, *77*, 76–91.

Huang, D., Tan, B., Yang, W., Shabanov, N. V., Knyazikhin, Y., & Myneni, R. B. (2004). Evaluation of collection 3 MODIS LAI products with respect to input data uncertainties—case study for grasses. *Remote Sensing of Environment* (submitted September 2003).

Knyazikhin, Y., Martonchik, J. V., Diner, D. J., Myneni, R. B., Verstraete, M., Pinty, B., & Gorbon, N. (1998b). Estimation of vegetation canopy leaf area index and fraction of absorbed photosynthetically active radiation from atmosphere-corrected MISR data. *Journal of Geophysical Research*, *103*, 32239–32256.

Knyazikhin, Y., Martonchik, J. V., Myneni, R. B., Diner, D. J., & Runing, S. (1998a). Synergistic algorithm for estimating vegetation canopy leaf area index and fraction of absorbed photosynthetically active radiation from MODIS and MISR data. *Journal of Geophysical Research*, *103*, 32257–32275.

Knyazikhin, Y., Mieben, G., Panfyorov, O., & Gravenhorst, G. (1997). Small-scale study of three dimensional distribution of photosynthetically active radiation in forest. *Agricultural and Forest Meteorology*, *88*, 215–239.

LI-COR. 1992. *LAI-2000 plant canopy analyzer instruction manual* (pp. 4–12).

MacDonald, R. B., & Hall, F. G. (1980). Global crop forecasting. *Science*, *208*, 670–679.

Markham, B. L., & Townshend, J. R. G. (1981). Landcover classification accuracy as a function of sensor spatial resolution. *Proceedings of the 15th international symposium on Remote Sensing of Environment held in Ann Arbor, Michigan, U.S.A.* (pp. 1075–1090). USA: ERIM.

Miller, J. B. (1967). A formula for average foliage density. *Australian Journal of Botany*, *15*, 141–144.

Morisette, J., Privette, J., & Justice, C. (2002). A framework for the validation of MODIS Land products,. *Remote Sensing of Environment*, *83*, 77–96.

Myneni, R. B., Hoffman, S., Knyazikhin, Y., Privette, J. L., Glassy, J., Tian, Y., Wang, Y., Song, X., Zhang, Y., Smith, G. R., Lotsch, A., Friedl, M., Morisette, J. T., Votava, P., Nemani, R. R., & Running, S. W. (2002). Global products of vegetation leaf area and fraction absorbed PAR from year one of MODIS data. *Remote Sensing of Environment*, *83*, 214–231.

Myneni, R. B., Knyazikhin, Y., Zhang, Y., Tian, Y., Wang, Y., Lotsch, A., Privette, J. L., Morisette, J. T., Running, S. W., Nemani, R., Glassy, J., & Votava, P., (1999). MODIS leaf area index (LAI) and fraction of photosynthetically active radiation absorbed by vegetation (FPAR) product (MOD15) algorithm theoretical basis document, Version 4.0 (p. 5).

Myneni, R. B., Nemani, R. R., & Running, S. W. (1997). Estimation of global leaf area index and absorbed PAR using radiative transfer models. *IEEE Transactions on Geoscience and Remote Sensing*, *35*, 1380–1393.

Nemani, R., Pierce, L., Running, S., & Band, L. (1993). Forest ecosystem process at the watershed scale: Sensitivity to remotely-sensed leaf area index estimates. *International Journal of Remote Sensing*, *14*, 2519–2534.

Peterson, D. L., Spanner, M. A., Running, R. W., & Band, L. (1987). Relationship of thematic mapper simulator data to leaf area index of temperate coniferous forest. *Remote Sensing of Environment*, *22*, 323–341.

Privette, J. L., Myneni, R. B., Knyazikhin, Y., Mukufute, M., Roberts, G., Tian, Y., Wang, Y., & Leblanc, S. G. (2002). Early spatial and temporal

validation of MODIS LAI product in Africa. *Remote Sensing of Environment*, *83*, 232–243.

Rahman, H., & Didieu, G. (1994). SMAC: A simplified method for the atmospheric correction of satellite measurements in the solar spectrum. *International Journal of Remote Sensing*, *15*, 123–143.

Running, S. W., Baldocchi, D., Turner, D., Gower, S., Bakwin, P., & Hibbard, K. (1999). A global terrestrial monitoring network integrating tower fluxes, flask sampling, ecosystem modeling and EOS data. *Remote Sensing of Environment*, *70*, 108–127.

Running, S. W., Peterson, D. L., Spanner, M. A., & Teuber, K. B. (1986). Remote sensing of coniferous forest leaf are. *Ecology*, *67*, 273–276.

Sellers, P. J., Randall, D. A., Betts, A. K., Hall, F. G., Berry, J. A., Collatz, G. J., Denning, A. S., Mooney, H. A., Nobre, C. A., Sato, N., Field, C. B., & Henderson-sellers, A. (1997). Modeling the exchanges of energy, water, and carbon between continents and the atmosphere. *Science*, *275*, 502–509.

Spanner, M., Johnson, L., Miller, J., McCreight, R., Freemantle, J., & Gong, P. (1994). Remote sensing of seasonal leaf area index across the Oregon Transect. *Ecological Applications*, *4*, 258–271.

Spanner, M. A., Pierce, L. L., Peterson, D. L., & Running, S. W. (1990). Remote sensing of temperate coniferous forest leaf area index. The influence of canopy closure, understory vegetation and background reflectance. *International Journal of Remote Sensing*, *11*, 95–111.

Stenberg, P. (1996). Correcting LAI-2000 estimates for the clumping of needles in shoots of conifers. *Agricultural and Forest Meteorology*, *79*, 1–8.

Tian, Y., Zhang, Y., Knyazikhin, Y., Myneni, R. B., Glassy, J. M., Dedieu, G., & Running, S. W. (2000). Prototyping of MODIS LAI and FPAR algorithm with LASUR and LANDSAT data. *IEEE Transactions on Geoscience and Remote Sensing*, *38*(5), 2387–2401.

Tian, Y., Wang, Y., Zhang, Y., Knyazikhin, Y., Bogaert, J., & Myneni, R. B. (2002a). Radiative transfer based scaling of LAI/FPAR retrievals from reflectance data of different resolutions. *Remote Sensing of Environment*, *84*, 143–159.

Tian, Y., Woodcock, C. E., Wang, Y., Privette, J. L., Shabanov, N. V., Zhou, L., Buermann, W., Dong, J., Veikkanen, B., Hame, T., Ozdogan, M., Knyazikhin, Y., & Myneni, R. B. (2002b). Multiscale analysis and validation of the MODIS LAI product over Maun, Botswana: I. Uncertainty assessment. *Remote Sensing of Environment*, *83*, 414–430.

Tian, Y., Woodcock, C. E., Wang, Y., Privette, J. L., Shabanov, N. V., Zhou, L., Buermann, W., Dong, J., Veikkanen, B., Hame, T., Ozdogan, M., Knyazikhin, Y., & Myneni, R. B. (2002c). Multiscale analysis and validation of the MODIS LAI product over Maun, Botswana: II. Sampling strategy. *Remote Sensing of Environment*, *83*, 431–441.

Turner, D. P., Cohen, W. B., Kennedy, R. E., Fassnacht, K. S., & Briggs, J. M. (1999). Relationships between leaf area index and Landsat TM spectral vegetation indices across three temperate zone sites. *Remote Sensing of Environment*, *70*, 52–68.

Wang, Y., Buermann, W., Stenberg, P., Smolander, H., Häme, T., Tian, Y., Hu, J., Knyazikhin, Y., & Myneni, R. B. (2003). Hyperspectral remote sensing of vegetation canopy: Leaf area index and foliage optical properties. *Remote Sensing of Environment*, *85*, 304–315.

Wang, Y., Tian, Y., Zhang, Y., El-Saleous, N., Knyazikhin, Y., Vermote, E., & Myneni, R. B. (2001). Investigation of product accuracy as a function of input and model uncertainties: Case study with SeaWiFS and MODIS LAI/FPAR algorithm. *Remote Sensing of Environment*, *78*, 296–311.

Woodcock, C. E., Collins, J. B., & Jupp, D. L. B. (1997). Scaling remote sensing models. In P. R. Van Gardingen, G. M. Foody, & P. J. Curran (Eds.), *Scaling-up from cell to landscape* (pp. 61–77). United Kingdom: Cambridge.

Woodcock, C. E., & Harward, V. J. (1992). Nested-hierarchical scene models and image segmentation. *International Journal of Remote Sensing*, *13*(16), 3167–3187.